Molecular dynamic simulation of dicarboxylic acid coated aqueous aerosol: structure and processing of water vapor

Xiaofei Ma,[a] Purnendu Chakraborty,[a] Brian J. Henz[c] and Michael R. Zachariah*[ab]

Organic monolayers at the surfaces of aqueous aerosols play an important role in determining the mass, heat transfer rate and surface reactivity of atmospheric aerosols. They can potentially contribute to the formation of cloud condensation nuclei (CCN) and are involved in a series of chemical reactions occurring in atmosphere. Recent studies even suggest that organic-coated interfaces could have played some role in prebiotic biochemistry and the origin of life. However, creating reproducible, well-characterized aqueous aerosol particles coated with organic films is an experimental challenge. This opens the opportunity for computer simulations and modeling of these complex structures. In this work, molecular dynamics simulation was used to probe the structure and the interfacial properties of the dicarboxylic acid coated aqueous aerosol. Low molecular weight dicarboxylic acids of various chain lengths and water solubility were chosen to coat a water droplet consisting of 2440 water molecules. For malonic acid coated aerosol, the surface acid molecules dissolved into the water core and formed an ordered structure due to the hydrophobic interactions. The acid and the water are separated inside the aerosol. For other nanoaerosols coated with low solubility acids, phase separation between water and acid molecules was observed on the surface of the particle. To study the water processing of the coated aerosols, the water vapor accommodation factors were calculated.

Introduction

Organic material is ubiquitous in the earth's atmosphere and represents an important fraction of the fine aerosol mass. Studies have shown that total organic carbon can represent 10–65% of the aerosol mass and exists as a complex mixture of hundreds of organic compounds, while secondary organic carbon can contribute up to 25–50% of the fine aerosol mass in urban polluted areas.[1] Indirectly, atmospheric aerosols can affect the radiative properties and lifetime of clouds and thus have an influence on global climate by acting as cloud condensation nuclei (CCN).[2] Observations have revealed that more than 60% of the CCN can consist of organic constituents.[3] Recent experimental studies and thermodynamic analysis of organic marine aerosols even suggest that atmospheric aerosols could act as prebiotic chemical reactors and play a role in the origin of life.[4,5] Despite the considerable fraction of organic matters in atmospheric aerosols and significant importance of their environmental and biological functions, little is known about their structure and influence on atmospheric processes.

The organic materials can be water-soluble and insoluble, volatile and nonvolatile, surface-active and surface-inactive, and biogenic and anthropogenic. Depending on their physical properties (*e.g.* solubility and volatility), the organics can form different structured films on existing aerosol particle surfaces. Water-insoluble organic molecules are likely to be closed-packed and oriented and thus tend to form "condensed films" on the particle surfaces. Phase transitions which correspond to differing degrees of ordering of the surfactant molecules can take place in those films.[6] Our previous molecular dynamic simulation results[7,8] on the structure of long-chain fatty acid coated nanoaerosols showed that in the final stage of equilibrium, an inverted micelle structure is formed, and consistent with a previously proposed "inverted micelle" model.[9] In this structure a water core is surrounded by surface adsorbed fatty acid molecules. On the other hand, water-soluble organic surfactant molecules tend to form less compact films which do not undergo phase transitions to more compact structures.

The primary relevance of these structures is how they subsequently interact with other organics, accommodation of water vapor, and its ability to act as cloud condensation nuclei. There is experimental evidence that organic compounds perturb the uptake of trace gases onto aqueous surfaces.[10] The presence of the organic films on water drops could significantly alter both condensation and evaporation rates. To complicate this already difficult problem, atmospheric "processing" of the surface by

[a] *Department of Mechanical Engineering and Department of Chemistry and Biochemistry, University of Maryland, College Park, MD 20742, USA. E-mail: mrz@umd.edu*
[b] *National Institute of Standards and Technology, Gaithersburg, MD 20899, USA*
[c] *U.S. Army Research Laboratory, Aberdeen Proving Ground, MD 21005, USA*

atmospheric oxidants would further alter the surface properties of the aerosol, leading to further changes in reactivity.[6,9]

Among the various kinds of organic compounds, low molecular weight dicarboxylic acids have attracted much attention due to their large prevalence and interesting physico-chemical properties. These types of acids have been identified as one of the major organics in both urban and rural areas and are a ubiquitous organic aerosol constituent in the marine and even Arctic atmosphere.[11,12] Observations have shown that dicarboxylic acids are also commonly found in the organic fraction of secondary aerosols. However, their formation and partition to the aerosol phase are still unclear. In biology, dicarboxylic acids are important metabolic products of fatty acids. During recent years, a considerable effort has been made to understand the properties of low molecular weight dicarboxylic acids (C3–C9). It is known that the physico-chemical properties of low molecular weight dicarboxylic acids such as solubility, vapor pressure, evaporation rate, melting and boiling points alternate with the number of carbon atoms.[13,14] Those physicochemical properties have profound effect on the CCN activity. One of the major questions surrounding organic compounds focuses on the changes in surface tension of the droplet due to the presence of the organic and the solubility of the compound.[2] Water-soluble materials are known to affect droplet activation by lowering the surface tension and thus changing the critical droplet radius. Experiments have confirmed that this effect can be well predicted by the Kohler theory for soluble inorganic species and organics that are wettable by water,[15] when the two components are homogenously dispersed. However, when considering extending the current theory, low-solubility organic species are equally important. The low molecular weight dicarboxylic acids (C3–C9) cover a wide range of solubility and thus provide an excellent platform to study the effect of solubility on the CCN activation.

With hydrophilic groups at both ends of a hydrophobic hydrocarbon chain, dicarboxylic acids are bolaamphiphilic molecules. The structure and phase behavior of these molecules in a particular type of medium are determined by unique intermolecular interactions: the hydrophobic inter-actions between hydrocarbon chains, the hydrophilic and/or the electrostatic interactions between the head groups. When amphiphilic molecules are dispersed in water, the hydrophobic interactions of the hydrocarbon chains drive the molecules to self-assemble into structures where the hydrophobic tails are shielded from unfavorable interactions with water by the hydrophilic, polar head groups.[16] Like amphiphilic molecules, bolaamphiphilic molecule aggregation is driven by hydrophobic interactions, which can form self-assembly structures, including, spherical lipid particles, vesicles produced from long-chain molecules, and micelles from short-chain, water-soluble bolaamphiphiles.[17] Not surprisingly compared with amphilic molecules, the introduction of a second hydrophilic head group generally induces a higher solubility in water and an increase in the critical micelle concentration.

Previous experiments have been carried out to investigate the cloud activity of various pure dicarboxylic acid aerosols from highly-soluble acids to almost insoluble acids.[11,15,18] The TDMA (Tandem DMA) method is frequently used in laboratory studies. In this method, the first DMA produces nearly monodisperse particles of a known size while the second DMA measures the particle size distribution of the final aerosol. However, there are some drawbacks associated with this method. First, the DMAs are designed for classifying spherical particles, and the results are interpreted based on a singly charged assumption. Therefore, depending on particle morphology, mass and cross-sectional area which affects the charging efficiency, there is a possibility that DMA could lead to incorrect size classification. Second, the ion-mobility method deals with the whole aerosol population, so it is impossible to use this method to monitor the water processing of individual particles. In fact, since molecular processes involve dynamics happening over short distances (nanometer length scale) and short times (nanoseconds time scale), these processes are difficult to probe experimentally. Furthermore, the atmospheric organic aerosols usually consist of more than one chemical species, and the organics can form complex structures such as monolayers, thin films on the aerosol surfaces. It is an experimental challenge to create reproducible, well-characterized aqueous aerosol particles which are coated with an organic film. However, on the other hand, the structure of complex aerosols can be explicitly defined in molecular simulations and the dynamics of the molecular-scale process can be followed explicitly as well.

In this work, we employed a molecular dynamic simulation method to study the structure evolution and water processing of various dicarboxylic acids coated water droplets. Two questions are addressed in our study: (1) What is the relation-ship between the aerosol final structure and physical properties of coated dicarboxylic acid molecules? (2) How does the aerosol structure affect the water processing of the coated aerosol?

Computational model and simulation details

The molecular dynamics simulations in this work were carried out using Lammps[19] (Large-scale Atomic/Molecular Massively Parallel Simulator, http://lammps.sandia.gov) a software package developed by Sandia National Laboratories.

1 Simulating the water core

For simulating the water molecule, we used the extended simple point charge (SPC/E) interaction potential developed by Berendsen et al.[20,21] This model consists of a total of three sites for the electrostatic interactions of water with an OH distance of 0.1 nm and HOH angle of 109.47°. The partial positive charges of +0.4328e on the hydrogen atoms are exactly balanced by partial negative charges of −0.8476e located on the oxygen atom. A pairwise Lennard-Jones inter-action centered on the oxygen atoms is used to compute the van der Waals forces between two water molecules. The expression is given by:

$$V_{LJ}(r_{ij}) = -\left(\frac{A}{r_{ij}}\right)^6 + \left(\frac{B}{r_{ij}}\right)^{12} \qquad (1)$$

with $A = 0.37122$ (kJ mol^{-1})$^{1/6}$ nm, $B = 0.3428$ (kJ mol^{-1})$^{1/12}$ nm, where r_{ij} is the distance between two oxygen atoms. The SPC/E

This journal is © the Owner Societies 2011

Phys. Chem. Chem. Phys., 2011, **13**, 9374–9384 | 9375

potential has been studied extensively. It can provide accurate reproduction of water surface tension and its temperature dependence[22] and the effects of simulation size and the treatment of long-range interactions on surface tension have been shown to be less than 10%.[23]

The first step toward building a dicarboxylic acid coated aqueous aerosol was to build a pure water droplet. The detailed procedures for preparing an equilibrated water droplet are described in our previous work.[7] In brief, the water droplet is evolved from a simple cubic lattice structure with the oxygen atom at the vertex of each cube. The initial sphere configuration consisting of 2440 water molecules was generated by considering only the water molecules inside a sphere of a certain radius. The water droplet is equilibrated at the temperature of 260 K. The SHAKE algorithm[24] was used to apply constraints between the O–H bond and H–O–H angle to maintain the rigidity of the water molecules. The radial distribution function confirms the liquid phase of the prepared water droplet.

2 Modeling the dicarboxylic acid molecule

The next step was to coat the spherical water droplet with dicarboxylic acid molecules. By identifying the surface molecules of the water droplet, we placed dicarboxylic acid molecules on the surface water sites with one of the carboxyl groups of the dicarboxylic acid attached to the surface water molecule and the straight chain of the dicarboxylic acid placed radially outward. The initial coating density is about 6.6 molecules per nm^2.

The dicarboxylic acids simulated were malonic acid (C3), succinic acid (C4), glutaric acid (C5), adipic acid (C6), pimelic acid (C7), suberic acid (C8), azelaic acid (C9) and branched azelaic acid (C9_branched). The physical properties of these dicarboxylic acids are summarized in Table 1. For modeling the dicarboxylic acid molecule, we used a mixture of the "fully atomistic" method and the "united atom" method. The high-accuracy/high computational requirement fully atomistic method is used to model the carboxyl group (–COOH group) while the less accurate/lower computational requirement united atom method is employed to simulate the methylene group (–CH$_2$ group). In the united atom setup, the number of interaction sites is reduced by subsuming some or all of the atoms into the atoms to which they are bonded. Thus considerable computation savings are possible. In our simulation, each methylene group (–CH$_2$ group) is represented by a single site with interactions defined between these sites. An example of the dicarboxylic acid in this work is shown in Fig. 1. During the simulation, the O–H bond in the carboxyl group was kept rigid using the SHAKE algorithm.
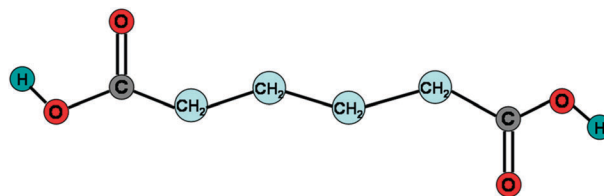

Fig. 1 Structure of a dicarboxylic acid (C6).

The reliability of predictions from molecular simulations is determined largely by the accuracy of the representation of the intermolecular interaction potentials. The potentials used in our model include nonbonded interactions between each pair of atoms and bonded interactions between bonded atoms which have contributions from bond stretching, angle vibration, proper and improper dihedral interactions. For non-bonded force calculation, the switched Lennard-Jones and the switched coulombic potential were used to simulate the van der Waals interactions and the electrostatic interactions, respectively. The switched forces are given by:

$$E = \begin{cases} \mathrm{LJ}(r) & r < r_{in} \\ S(r) \cdot \mathrm{LJ}(r) & r_{in} < r < r_{out} \\ 0 & r > r_{out} \end{cases}$$

$$E = \begin{cases} C(r) & r < r_{in} \\ S(r) \cdot C(r) & r_{in} < r < r_{out} \\ 0 & r > r_{out} \end{cases} \quad (2)$$

$$\mathrm{LJ}(r) = 4\varepsilon \left[\left(\frac{\sigma}{r} \right)^{12} - \left(\frac{\sigma}{r} \right)^{6} \right]$$

$$C(r) = \frac{Cq_i q_j}{\varepsilon r}$$

$$S(r) = \frac{[r_{out}^2 - r^2]^2 [r_{out}^2 + 2r^2 - 3r_{in}^2]}{[r_{out}^2 - r_{in}^2]^3}$$

Harmonic potentials of the form $E = K(x - x_0)^2$ (where K is a prefactor, x is the position vector or angle and x_0 is the corresponding equilibrium value) were chosen to model bond stretching and angle vibrations. The periodic function $E = K[1 + \cos(n\phi - d)]$ was used to describe the proper dihedral interactions. For the improper interactions, a harmonic potential $E = K(\chi - \chi_0)^2$ was chosen to keep a planar group in the same plane. The potential parameters used in these simulations were obtained from the Gromacs force field database and are listed in Table 2.

Table 1 Physical properties of the dicarboxylic acids studied in this work

Dicarboxylic acid	Chemical formula	Molar mass/g mol^{-1}	Density/g cm^{-3} [2,11,14]	Solubility in water/ g per 100 g water[2,11]
Malonic acid (C3)	HOOC–(CH$_2$)–COOH	104.06	1.631	161
Succinic acid (C4)	HOOC–(CH$_2$)$_2$–COOH	118.09	1.572	8.8
Glutaric acid (C5)	HOOC–(CH$_2$)$_3$–COOH	132.12	1.424	116
Adipic acid (C6)	HOOC–(CH$_2$)$_4$–COOH	146.14	1.360	2.5
Pimelic acid (C7)	HOOC–(CH$_2$)$_5$–COOH	160.17	1.281	71
Suberic acid (C8)	HOOC–(CH$_2$)$_6$–COOH	174.20	1.272	0
Azelaic acid (C9)	HOOC–(CH$_2$)$_7$–COOH	188.22	1.251	0

3 Equilibration procedures

After attaching a monolayer dicarboxylic acid to the surface of the water droplet, an energy minimization run was performed using the conjugate gradient (CG) algorithm to relax the initial configuration containing highly overlapped atoms. The system was then allowed to equilibrate at 0 K for 10 ps using constant NVE integration with the velocity-Verlet algorithm to update position and velocity for all atoms. A timestep of 1 fs was typically chosen to ensure energy conservation. During the equilibration process, the temperature was controlled by rescaling the velocities every timestep. After the system relaxation at 0 K, the coated particle was slowly heated to 260 K over 200 ps and then allowed to equilibrate for 400 ps. Following that, the system was heated to 300 K and allowed to equilibrate at that temperature for up to 8 ns. For the final step of the preparation process, the simulations were switched from a constant temperature to a constant energy calculation to ensure that the average system temperature did not deviate by more than 10 K. The simulations were carried out in a constant energy environment during the data generation phase. All the simulations were run on a Linux cluster, running in parallel on 8 processors.

Table 2

(1) Nonbonded force parameters

Atom	ε/kcal mol^{-1}	σ/Å
OW–OW	0.1553	3.166
HW1–HW1	0.0	0.0
HW2–HW2	0.0	0.0
HO–HO	0.0	0.0
OA–OA	0.2029	2.955
C–C	0.0970	3.361
O–O	0.4122	2.6260
CH$_2$–CH$_2$	0.1400	3.9647

(2) Harmonic bond parameters

Bond	K/kcal mol^{-1} Å^{-2}	r_0/Å
OW–HW1; OW–HW2	0.0	1.0
HO–OA	375.0	1.0
OA–C	450.0	1.36
C=O	600.0	1.23
C–CH$_2$; CH$_2$–CH$_2$	400.0	1.53

(3) Harmonic angle parameters

Angle	K/kcal mol^{-1} rad^{-2}	θ_0/°
HW1–OW–HW2	0.0	109.47
HO–OA–C	47.5	109.5
OA–C=O	60.0	124.0
OA–C–CH$_2$	60.0	115.0
O=C–CH$_2$	60.0	121.0
C–CH$_2$–CH$_2$; CH$_2$–CH$_2$–CH$_2$	55.0	111.0

(4) Proper dihedral parameters

Dihedral	K/cal mol^{-1}	n (integer)	d/°
HO–OA–C–CH$_2$; HO–OA–C=O	4.0	2	180
OA–C–CH$_2$–CH$_2$; O=C–CH$_2$–CH$_2$	0.1	6	0
C–CH$_2$–CH$_2$–CH$_2$; CH$_2$–CH$_2$–CH$_2$–CH$_2$	1.4	3	0

(5) Improper dihedral parameters

Improper dihedral	K/cal mol^{-1} rad^{-2}	χ_0/°
C OA CH$_2$ O	40	0.0

Our mixture method is computationally more efficient than the fully atomistic method yet provides sufficient accuracy for the analysis.

Results and discussion

In this section, the results from the molecular dynamics simulations are presented and discussed. In order to study the effect of dicarboxylic acid chain length on the structure of coated nanoaerosols, we computed several physical properties, including the radial density distributions, diffusion coefficients and radial distribution functions. In order to study water vapor processing of the coated nanoaerosols, water molecules were impinged on the surface with a Boltzmann energy distribution to obtain thermal sticking coefficients.

1 Structure

The time evolution of different dicarboxylic acids coated nanoaerosol structures were monitored during the simulation process. Different equilibrium morphologies were observed. For C3-coated nanoaerosol, the C3 molecules slowly migrate from the surface to the core of the nanoaerosol. This seems to occur in two states. In the first ∼1 ns, the C3 molecules dissolve and are dispersed inside the water droplet. By 5–6 ns, however the dispersed C3 molecules dissolve further into the water core and assemble around the center of the nanoaerosol. The initial and final morphologies of C3-coated nanoaerosol are presented in Fig. 2(a).

The evolution paths of C5–C9 coated nanoaerosols are essentially similar to each other but significantly different from that of C3-coated nanoaerosol. As a representative system, we present the initial and final morphologies of C8-coated nanoaerosol in Fig. 2(b). Unlike C3 molecules, C8 molecules cannot dissolve into the water droplet. The result is phase separation leading to the acid molecules segregation to one side of the droplet, and forming a multilayer structure, similar to what might be expected for the separation of oil and water. This behavior was observed for C5–C9 coated nanoaerosols. Apparently, for sufficiently long molecules the combined effects of the acid–acid interaction with the hydrocarbon backbone interactions are more competitive than the acid–water interaction. The equilibrated structure of C4-coated nanoaerosol is found to intermediate between the C3 and C8 cases with some of the acid molecules dissolved into the water core while the rest formed a separate acid cluster.

To investigate the effect of a branched chain on the structure evolution of dicarboxylic acid coated nanoaerosol, a C9 molecule was modified to add two side CH$_3$ groups. Fig. 2(c) shows the initial and final structures of the system. A schematic of the branched acid structure is also shown in Fig. 2(c). Different from previous cases, the C9_branched acid molecules did not dissolve into the water droplet or form a separate acid cluster, but rather maintained the initial inverted micelle structure. Apparently, the addition of a side group actually stabilizes the monolayer, by constraining the molecular conformation to a linear structure.
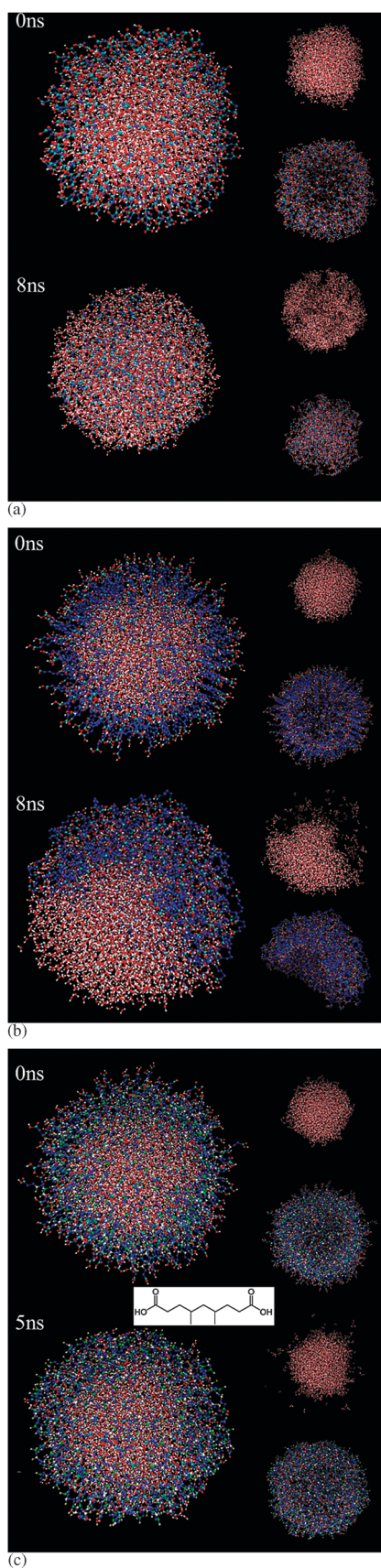
Fig. 2 Structures of dicarboxylic acid coated nanoaerosols: (a) structure of C3 coated nanoaerosol, (b) structure of C8 coated nanoaerosol, (c) structure of C9_branched coated nanoaerosol (c).

2 Radial density

The density profiles of the dicarboxylic acid coated nanoaerosols were calculated as a function of radial distance r. To calculate density, we considered a shell of thickness δr at a distance r from the center of mass. The density at a radial distance r is given by the mass of all the sites in that shell divided by the volume of the shell. Due to the lack of spherical symmetry, the density calculation could not be performed on C4–C9 dicarboxylic acid coated nanoaerosols. The calculated density profiles for C3 and C9_branched dicarboxylic acid coated nanoaerosols are presented in Fig. 3.

The density profiles for the C3 acid coated nanoaerosol show, in Fig. 3(a), the acid density distribution gradually shifting to the inside of the aerosol. After about 5–6 ns of equilibration, both water and acid density profiles converge to their equilibrium values. Curiously the water density shows a bimodal distribution, but overall the structure would indicate that the surface is enriched in water relative to the interior of the droplet. On the other hand the density profiles of C9_branched acid coated nanoaerosol (Fig. 3(b)) maintain a core-shell structure.

3 Radial distribution function

The radial distribution function (RDF), $g(r)$, is defined as the number of atoms a distance r from a given atom compared with the number of atoms at the same distance in an ideal gas. In our simulation, the RDF for each atom pair is histogrammed into 100 bins from distance 0 to the maximum force cutoff distance. To investigate the microstructure changes of the dicarboxylic acid coated nanoaerosols, RDFs between different atom pairs were calculated. The RDF of the water oxygen–oxygen pair is a good indicator of changes in the water structure and RDF for water oxygen and the carbon in the acid head group, tracks the interaction between water and acid. Finally the RDF of the acids central CH_2–CH_2 groups characterizes the interaction between dicarboxylic acid molecules.

Fig. 4(a) shows the water oxygen–oxygen RDFs for C3, C8 and C9_branched acid coated nanoaerosols after equilibration. For all three RDFs, the major peak occurs at roughly 2.8 Å which is the well-known average hydrogen bond length in water. Fig. 4(b) compares the RDFs of the central CH_2–CH_2 groups for the three representative nanoaerosols after equilibration. The RDF for the C3 case exhibits a well resolved peak at around 5 Å, while the RDFs for C8 and C9_branched chains are much more diffuse. The reader is reminded that in the final equilibrium stage, the coating C3 acid molecules all dissolved into the water core. Thus, a clear peak in the RDF indicates that the C3 acid molecules apparently form a short-range ordered structure within the water core. The time evolution of the RDFs of acid central CH_2–CH_2 in the C3 case is presented in Fig. 5(a). The system starts from an initial "ordered structure" where all the acid molecules are pointing radially out of the water droplet, after 1 ns of equilibration, the acid molecules dissolve into the water droplet. This leads to the decrease in the peaks of RDF at 1 ns. As the system continually evolves, the peaks in RDFs grow which indicates the formation of a more ordered acid structure in water. To investigate the relative orientation
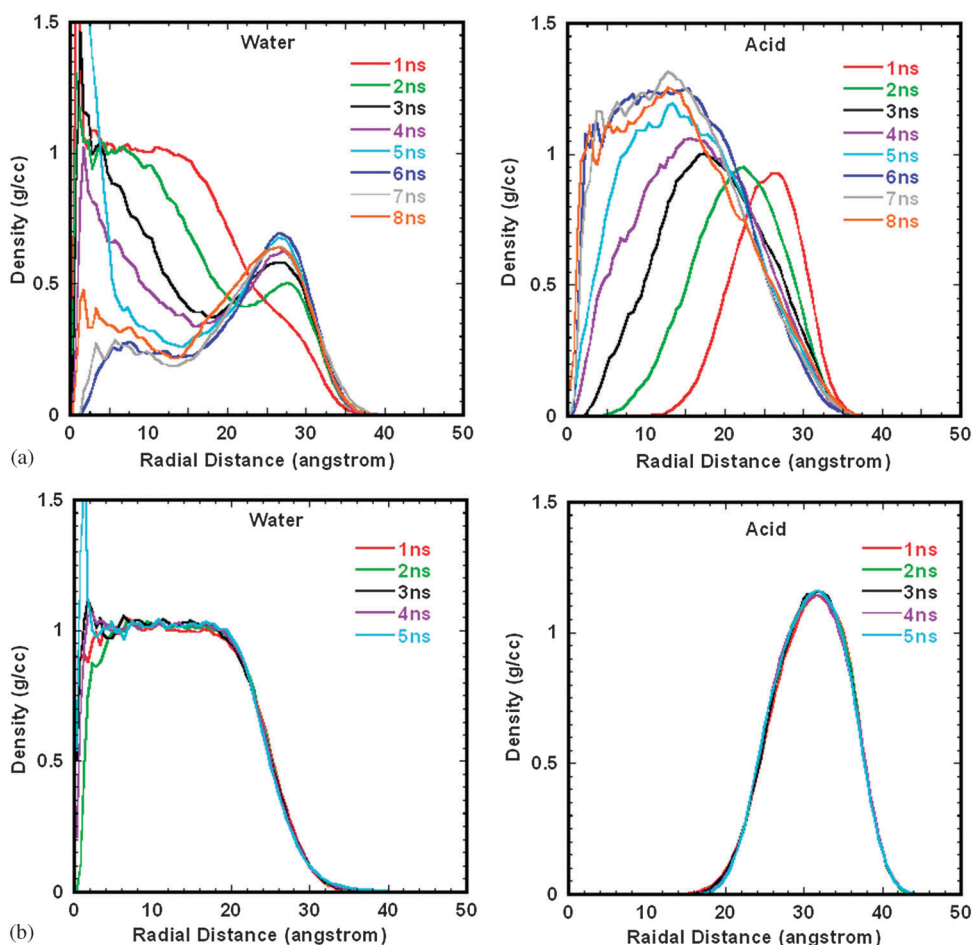
9378 | *Phys. Chem. Chem. Phys.*, 2011, **13**, 9374–9384

This journal is © the Owner Societies 2011

Fig. 3 Radial density distributions of (a) C3 and (b) C9_branched acids coated nanoaerosols as a function of simulation time.

between the C3 acid molecules, RDFs of different groups within the acid molecule are calculated both for the initial configuration and for the equilibrated structure. The results are presented in Fig. 5(b) (initial structure) and Fig. 5(c) (equilibrated structure). In Fig. 5(b), groups 1, 2 and 3 represent the carbon atom in the head group, CH_2 group, and the carbon atom in the tail group for a C3 molecule, respectively. As we can see from Fig. 5(b), the RDF for group 1 atoms has the highest peak intensity, while the RDF for group 3 atoms has the lowest peak intensity, which reflects the initial "radially outward" molecular configurations of C3 molecules. After equilibration, the RDFs for group 1 atoms and group 3 atoms almost overlap which indicates a equal separation between the group 1 atoms and group 3 atoms. The RDF for group 2 atoms peaks at a slightly large separation. This suggests a pairwise parallel configuration between C3 molecules (as shown in the inset of Fig. 5(c)) with the separation between the central CH_2 groups slightly larger than that for the head and tail groups.

To investigate the phase separation occurring in long chain dicarboxylic acids coated nanoaerosols, the RDFs of the atom pair between the water oxygen and the carbon atom in the acid head group for the C8 case were calculated at different stages of equilibration. The results are presented in Fig. 6. As we can see from the figure, starting from the initial "ordered configuration",

the peaks in the RDFs continuously decrease, indicating the increased separation between water and acid molecules.
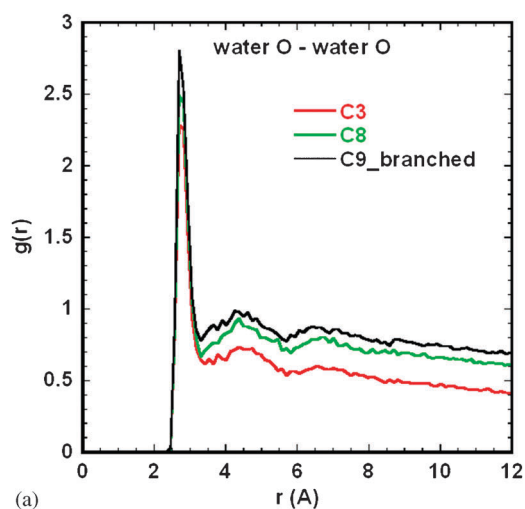
4 Phase separation mechanism

In order to study the phase separation of the long chain acids in more detail, a low surface coverage (0.6 molecules per nm^2), C8 coated nanoaerosol was prepared and allowed to evolve from an initial 'inverted micelle' configuration. The images of structure evolution of this nanoaerosol are presented in Fig. 7.
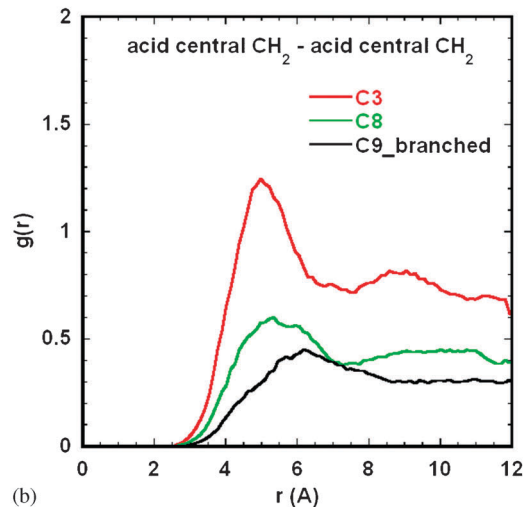
As can be seen from Fig. 7, the phase separation process between the acid and water molecules occurs in several stages. In the first stage, the C8 dicarboxylic acid molecules flop down onto the water droplet surface to maximize interaction between the two acid groups and water (0.1 ns–1 ns). The next stage of the phase separation process is the aggregation of the acid molecules. Here the dicarboxylic acid surface diffuses and aggregates to form multi-layered clusters of acid molecules which favor acid–acid interactions (1 ns–2.5 ns). In turn these clusters also surface diffuse to aggregate into larger clusters.

5 Discussion: hydrophobicity and the structure of dicarboxylic acid coated aqueous aerosol

The hydrophobic effect is the tendency for non-polar molecules and water to segregate, and is an important driving force for

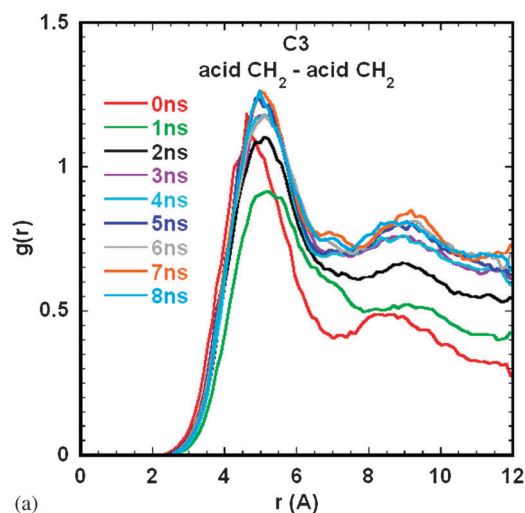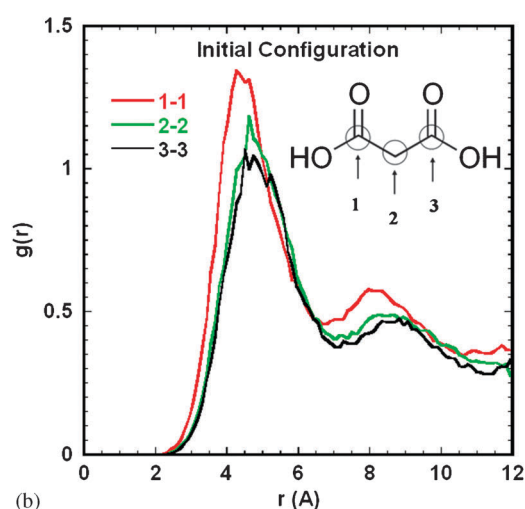**Fig. 4** RDFs for different atom pairs for C3, C8 and C9_branched dicarboxylic acid coated nanoaerosols. (a) RDFs of water O–water O and (b) RDFs of acid central CH_2–CH_2 groups.

amphiphlies self-assembly and biological folding.[25] Trying to mix hydrophobic molecules with water requires a decrease in hydrogen bonding, which if not energetically favored, just results in segregation of non-polar molecules from water, and an effective attraction between hydrophobic molecules.[26] If the hydrophobic molecule is small enough, such that the disruption of the hydrogen bond network is also small, then water molecules can adopt orientations to go around the small hydrophobic solute without sacrificing hydrogen bonds, or move away from the large hydrophobic object and form an interface around it.[27] The critical length scale dividing large hydrophobic units from small has been estimated to be ∼1 nm.[27]
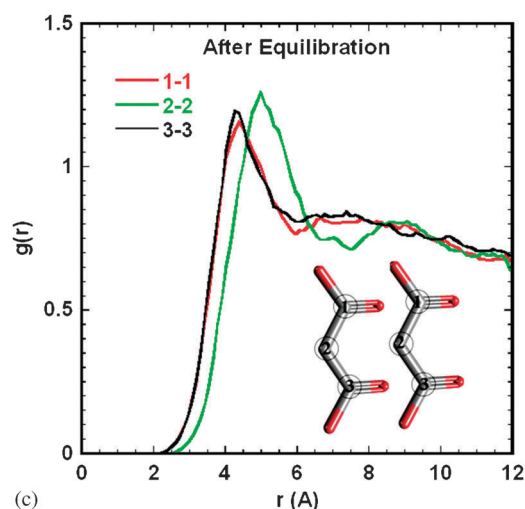
The dicarboxylic acid molecules studied in this work contain a hydrophobic hydrocarbon chain, which can participate in the hydrophobic interaction with water. The hydrophilic parts of the dicarboxylic acid molecules are not directly responsible for hydrophobic assemblies, but they can affect the arrangement of these assemblies relative to interfaces and other structures. The structures observed in our simulation for different dicarboxylic acid coated nanoaerosols can be explained successfully using the

Fig. 5 (a) Time evolution of the RDFs of acid central CH_2–CH_2 in the C3 case, (b) RDFs of atom groups within acid molecules at the initial configuration; the inset shows the grouping of atoms for a C3 molecule, (c) RDFs of atom groups within acid molecules after the equilibration process; the inset shows a cartoon of the pairwise parallel configuration between C3 molecules.

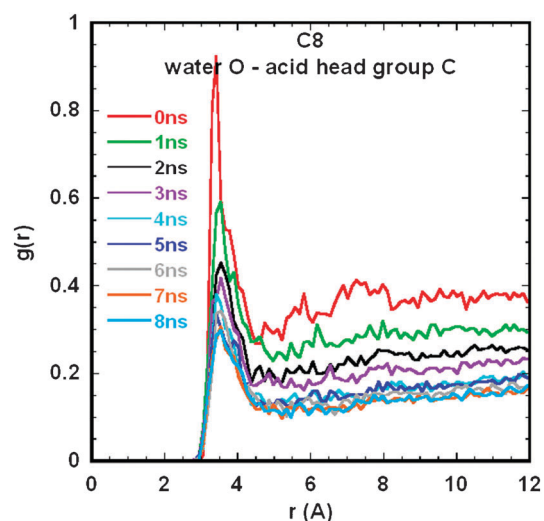knowledge of hydrophobic interactions between the acid molecules and the water molecules.

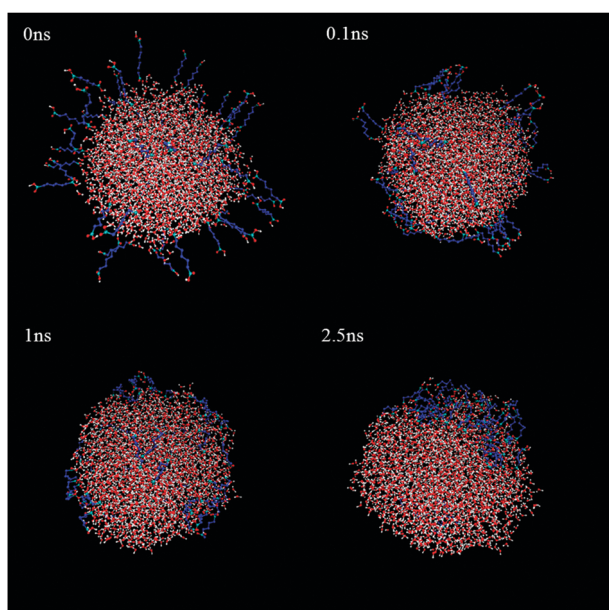**Fig. 6** RDFs of water O-acid head group C for C8 coated nanoaerosol at different equilibration stages.

Fig. 7 Phase separation of low coverage (0.6 molecules per nm^2), C8 acid coated nanoaerosol.

For C3 acid coated nanoaerosol, we observed a final structure with the surface acid molecules completely dissolved within the water core to form an ordered cluster (see $g(r)$ in Fig. 4(b)) at the center of the water droplet. As a result, the original water molecules at the droplet center were excluded, leading to a very low water density at the center (see Fig. 3(a)). This structure is readily understood in terms of the dependence of hydrophobic solvation on the size of hydrophobic unit. When the C3 acid molecules cluster together they form a sufficiently large hydrophobic unit (*i.e.* large volume to surface ratio), so that the salvation free energy of the acid cluster is lower than the overall salvation free energy of the individual acid molecules. By forming a nearly spherical acid cluster, the total acid surface area exposed to the unfavorable hydrophobic interactions with water is thus minimized. The diameter of this

acid cluster is about 2 nm which is consistent with the criteria that above 1 nm the energetic cost of assembling hydrophobic units is significantly more favorable than the entropic cost of keeping them separate.[25]

For nanoaerosols coated with low solubility dicarboxylic acids, we observed phase separation between acid and water at the surface of the water droplet with the acid molecules forming a layered aggregate. The radial distribution of the acid aggregate reveals that this aggregate structure is less ordered than the cluster structure formed by C3 acid molecules in water. Since the free energetic cost of dissolving large dicarboxylic acid molecules in water is formidable, the acid molecules will stay on the water droplet surface. However, as we can see from Fig. 6, due to the two hydrophilic head groups, the first step towards acid molecule aggregation is that each individual acid molecule folds on the surface of water droplet. This configuration is not energetically favorable since the hydrocarbon chain in each dicarboxylic acid molecule is close to the water. The equilibration process is to minimize this unfavorable interaction, by minimizing the total acid surface area exposed to water, resulting in aggregation. Since this aggregation process happens near the surface of water droplet, without water medium around the acid aggregate the hydrophobic interaction is not as strong as that in water. Therefore, the final structure of acid aggregate is less ordered than the structure of the C3 acid cluster in water.

For the high surface coverage (6.6 molecules per nm^2), C9_branched acid coated nanoaerosol, with the addition of a branched chain, the C9_branched acid molecule is hard to fold completely on the water surface due to the geometric constraints. Thus, the hydrophobic part of the acid molecule is not affected by the unfavorable interaction with water. The initial structure of C9_branched acid coated nanoaerosol keeps intact. However, for a low surface coverage C9_branched acid coated nanoaerosol, we do observe the phase separation between the acid and the water molecules, since in this case the acid molecules can fold on the surface of water droplet. Fig. 8 compares the initial and equilibrated configurations of a low surface coverage (0.6 molecules per nm^2) C9_branched acid coated nanoaerosol. A phase separation can be clearly seen.

6 Diffusion

In order to gain a better understanding of the dicarboxylic acid coating and how it interacts with the water droplet, we computed the diffusion coefficients for the dicarboxylic acid molecules and the water molecules. This is achieved by computing the mean square displacement of the dicarboxylic acid and water molecules in the simulation and evaluating the diffusion coefficient using eqn (3):

$$\frac{\partial \langle r^2(t) \rangle}{\partial t} = 2dD \qquad (3)$$

where $\langle r^2(t) \rangle$ is the mean square displacement (MSD) of the molecules being tracked, t is time, d is the dimension available for diffusion (in our case 3), and D is the diffusion coefficient. The calculated diffusion coefficients for different dicarboxylic acid molecules are presented in Fig. 9 as a function of molecular weight. The best-fit line of the calculated self-diffusion coefficients shows a (molecular weight)$^{-1}$ dependence, which is consistent
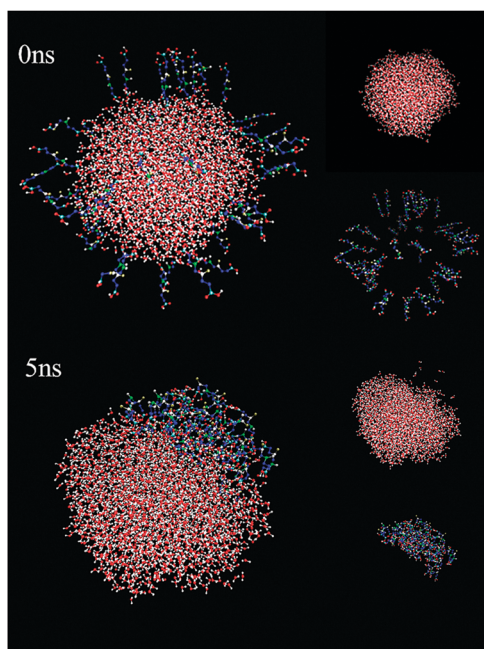
Fig. 8 Phase separation of a low surface coverage (0.6 molecules per nm^2), C9_branched acid coated nanoaerosol.
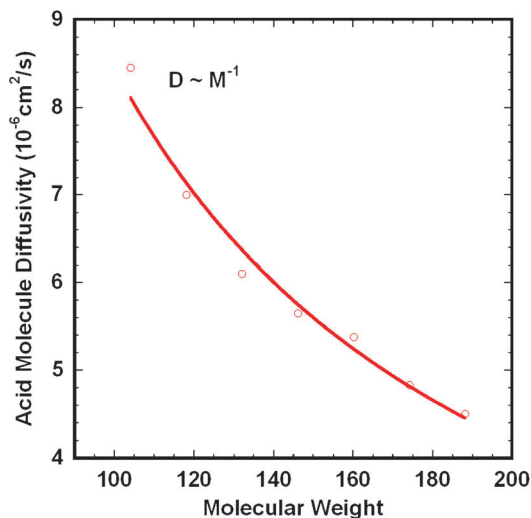

Fig. 9 Dicarboxylic acid diffusion coefficient as a function of molecular weight. The solid line is a curve fit to a (molecular weight)$^{-1}$ dependence.

with the Rouse model[28] which makes a "no entanglements" assumption, which is likely true for the relatively small acids being considered here. Interestingly the same molecular weight dependence on the diffusion coefficient applies for both the water soluble (C3 and C4) and non-soluble (C5–C9) molecules. The reader is reminded that the C3 acid molecules are fully dissolved into the water core and the C4 acid molecules are partially dissolved into the water. While for the longer chain acid molecules, a close-packed cluster phase is formed on the surface of the water droplet. However, in each case the acid molecules form a separate cluster either within the water droplet (C3, C4) or on the surface of water droplet (C5–C9). Therefore, the acid molecule self-diffusion process is

within the "bulk" acid materials. Interestingly, even though the clusters formed by the acid molecules constitute only a few hundreds of acid molecules (about 500 acid molecules), the calculated self-diffusion coefficient reflects only the contribution from bulk diffusion. Surface diffusion is apparently not an important factor here.

The diffusion coefficients for water molecules in different aerosol structures were also calculated and found to be essentially independent of the structure, with an average water diffusion coefficient of $\sim 3.5 \times 10^{-5}$ cm^2 s^{-1} at 300 K.

7 Water vapor processing

Finally we turn our attention to how these materials might act in the atmosphere. The accommodation of water vapor to liquid water surfaces plays an important role in the growth of cloud condensation nuclei into cloud droplets. Molecular simulations of water uptake on the vapor/liquid interface of water have been extensively studied.[10,29–33] However, there are only a few studies that have probed the effect of organic layers on the aqueous aerosol properties.[7,8] No surprising it is widely believed that composition, concentration, structure and surface properties of the organic coating all play a role in the water vapor evaporation from, and condensation to such aerosols. While some experiments have shown that surfactant films reduce the rate of evaporation of water,[34] others show for example that butanol coatings of up to 80% monolayer coverage do not seem to inhibit the water vapor evaporation.[35] Thus considerable uncertainty exists on the effects of organic layers on the uptake of atmospheric trace species.

In order to obtain a better understanding of the effect of dicarboxylic acid coating on the aerosol water vapor processing, the water sticking (mass accommodation) coefficient α was calculated for each coated nanoaerosol system. The sticking coefficient describing the probability of gas molecules being incorporated into aerosol is defined as:

$$\alpha = \frac{\text{number of molecules absorbed into the aerosol}}{\text{number of molecules impinging the aerosol surface}} \quad (4)$$

An accurate determination of the water sticking coefficient is important in predicting the nucleation and growth kinetics of cloud droplets.

To evaluate the water sticking coefficient, we placed water monomers outside the aerosol with a random velocity pointing to the aerosol surface, and counted the fraction at a given thermal velocity that would be absorbed. For each simulation, a single water molecule was placed randomly at a distance of 5 nm from the center of the nanoaerosol, and outside the potential cutoff distance so that initially no force was acting between the water monomer and the coated aerosol. The water molecule was then given an initial velocity pointing towards the center of the aerosol which is drawn from the Maxwell–Boltzmann speed distribution at 300 K. The trajectory of this water monomer was monitored for 100 ps. The water monomer was considered trapped in the aerosol if the distance between the monomer and the coated aerosol is smaller than the size of the aerosol, otherwise, it was considered non-absorbed. More than 60 such water trajectories were computed for each coated aerosol. The water sticking coefficient was then calculated as the ratio of number of absorbed monomers to the number of
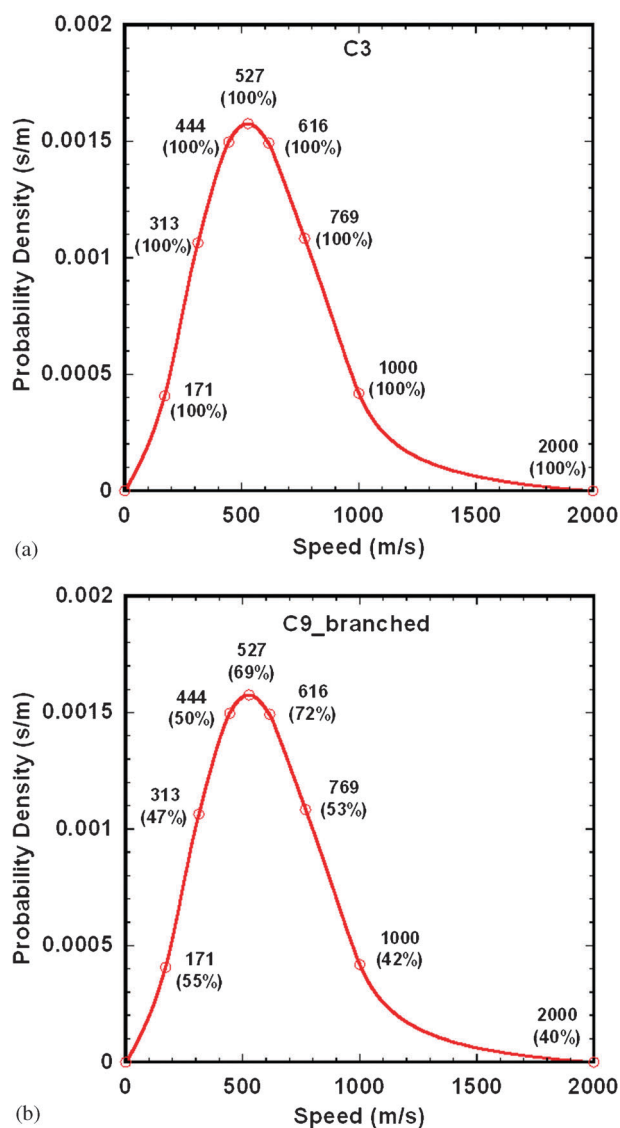
Fig. 10 Water vapor sticking coefficient for different coated nanoaerosols.

impinging monomers. The sticking coefficients were calculated for all the structures.

Fig. 10 presents the results of sticking coefficients calculation for different coated structures. As we can see from Fig. 10(a), the water sticking coefficient for C3_coated nanoaerosol is essentially unity at all impinging velocities. Since we have also seen that the C3 molecule moves to the core, the surface of this droplet is essentially water and thus should behave like a pure water droplet. Our result is consistent with other researchers' works[31,33,36] on pure water droplets showing a mass accommodation (condensation) coefficient of ~ 1. Fig. 10(b) shows the sticking coefficient calculation results for C9_branched acid coated nanoaerosol. As we can see from the figure, the sticking coefficient is the largest for incident speeds around the most probable speed and smaller at both lower and higher speeds. Compared with a pure water droplet, the sticking coefficient for C9_branched acid coated nanoaerosol is reduced, which indicates that the acid coating impedes the mass transfer from the gas phase to the aerosol phase. However, the C9_branched acid coated nanoaerosol

can still process water vapor. The sticking coefficients are as high as 70% around the most probable speeds. This is due to the apparent hydrophilic property of the surface of the coated nanoaerosol since the hydrophilic tails of C9_branched acids are all exposed to the environment. This water processing, however does not lead to absorption within the water core. Rather the processed water is associated with the hydrophilic tail of the C9_branched acids, over the timer period of the simulation. This is in contrast to our prior work on straight chain fatty acids which were shown to process the water to the core.

Because the longer chain dicarboxylic acid molecules are not homogeneously dispersed over the droplet surface we counted separately the water trajectories incident onto the water phase from the water trajectories incident onto the acid phase. As expected, the calculated sticking coefficient for water on water was essentially unity. However, for the water molecules impinging on the acid, almost all of them were reflected back to the gas phase, leading to a sticking coefficient close to zero. This result is consistent with the acid molecules forming a thick hydrophobic layered structure.

Conclusions

In this work, molecular dynamics simulations were used to probe the structure and the interfacial properties of dicarboxylic acid coated aqueous aerosol. Low molecular weight dicarboxylic acids of various chain lengths and water solubility (from malonic acid to azelaic acid) were chosen to coat a water droplet. The starting point of the coated aerosol is an inverted micelle model. For malonic acid coated aerosol, the original surface acid molecules dissolved into the water core. For other nanoaerosols coated with low solubility acids, phase separation between water and acid molecules was observed during the equilibration process. The detailed phase separation mechanism was investigated by monitoring the structure evolution of a 10% surface acid covered nanoaerosol.

Water vapor accommodation showed that for the C3 acid coated nanoaerosol, a water vapor accommodation factor of 1 was found for all incident water velocities. For longer chain coated nanoaerosols, due to the surface phase separation, a 100% sticking probability was found for water monomer colliding onto the water phase of the coated aerosol and an almost 0% sticking probability was found for water monomer colliding onto the acid phase.

Acknowledgements

References

1 C. N. Cruz and S. N. Pandis, A study of the ability of pure secondary organic aerosol to act as cloud condensation nuclei, *Atmos. Environ.*, 1997, **31**(15), 2205–2214.
2 N. C. Shantz, W. R. Leaitch and P. F. Caffrey, Effect of organics of low solubility on the growth rate of cloud droplets, *J. Geophys. Res.*, 2003, **108**(D5), 4168, DOI: 10.1029/2002JD002540.

3 B. Ervens, G. Feingold, S. L. Clegg and S. M. Kreidenweis, A modeling study of aqueous production of dicarboxylic acids: 2. Implications for cloud microphysics, *J. Geophys. Res.*, 2004, **109**(D15), D15206, DOI: 10.1029/2004JD004575.

4 D. J. Donaldson, H. Tervahattu, A. F. Tuck and V. Vaida, Organic aerosols and the origin of life: An hypothesis, *Origins Life Evol. Biospheres*, 2004, **34**(1/2), 57–67.

5 C. M. Dobson, G. B. Ellison, A. F. Tuck and V. Vaida, Atmospheric aerosols as prebiotic chemical reactors, *Proc. Natl. Acad. Sci. U. S. A.*, 2000, **97**(22), 11864–11868.

6 D. J. Donaldson and V. Vaida, The influence of organic films at the air-aqueous boundary on atmospheric processes, *Chem. Rev.*, 2006, **106**(4), 1445–1461.

7 P. Chakraborty and M. R. Zachariah, Sticking coefficient and processing of water vapor on organic-coated nanoaerosols, *J. Phys. Chem. A*, 2008, **112**(5), 966–972.

8 P. Chakraborty and M. R. Zachariah, "Effective" negative surface tension: A property of coated nanoaerosols relevant to the atmosphere, *J. Phys. Chem. A*, 2007, **111**(25), 5459–5464.

9 G. B. Ellison, A. F. Tuck and V. Vaida, Atmospheric processing of organic aerosols, *J. Geophys. Res.*, 1999, **104**(D9), 11633–11641.

10 C. E. Kolb, R. A. Cox, J. P. D. Abbatt, M. Ammann, E. J. Davis, D. J. Donaldson, B. C. Garrett, C. George, P. T. Griffiths, D. R. Hanson, M. Kulmala, G. McFiggans, U. Poschl, I. Riipinen, M. J. Rossi, Y. Rudich, P. E. Wagner, P. M. Winkler, D. R. Worsnop and C. D. O'Dowd, An overview of current issues in the uptake of atmospheric trace gases by aerosols and clouds, *Atmos. Chem. Phys.*, 2010, **10**(21), 10561–10605.

11 M. Hori, S. Ohta, N. Murao and S. Yamagata, Activation capability of water soluble organic substances as CCN, *J. Aerosol Sci.*, 2003, **34**(4), 419–448.

12 K. Kawamura, R. Semere, Y. Imai, Y. Fujii and M. Hayashi, Water soluble dicarboxylic acids and related compounds in Antarctic aerosols, *J. Geophys. Res.*, 1996, **101**(D13), 18721–18728.

13 M. Z. H. Rozaini and P. Brimblecombe, The odd–even behaviour of dicarboxylic acids solubility in the atmospheric aerosols, *Water, Air, Soil Pollut.*, 2008, **198**(1–4), 65–75.

14 M. Bilde, B. Svenningsson, J. Monster and T. Rosenorn, Even–odd alternation of evaporation rates and vapor pressures of C3–C9 dicarboxylic acid aerosols, *Environ. Sci. Technol.*, 2003, **37**(7), 1371–1378.

15 T. M. Raymond and S. N. Pandis, Cloud activation of single-component organic aerosol particles, *J. Geophys. Res.*, 2002, **107**(D24), 4787, DOI: 10.1029/2002JD002159.

16 S. A. Safran, *Statistical Thermodynamics of Surfaces, Interfaces, and Membranes*, Addison-Wesley Pub., Reading, Mass, 1994.

17 A. H. Fuhrhop and T. Y. Wang, Bolaamphiphiles, *Chem. Rev.*, 2004, **104**(6), 2901–2937.

18 C. E. Corrigan and T. Novakov, Cloud condensation nucleus activity of organic compounds: a laboratory study, *Atmos. Environ.*, 1999, **33**(17), 2661–2668.

19 S. Plimpton, Fast parallel algorithms for short-range molecular-dynamics, *J. Comput. Phys.*, 1995, **117**(1), 1–19.

20 H. J. C. Berendsen, J. R. Grigera and T. P. Straatsma, The missing term in effective pair potentials, *J. Phys. Chem.*, 1987, **91**(24), 6269–6271.

21 H. C. Berendsen, J. P. M. Postma, W. F. van Gunsteren and J. Hermans, Interaction Models for Water in Relation to Protein Hydration, in *Intermolecular Forces*, ed. B. Pullman, Reidel, Dordrecht, The Netherlands, 1981, pp. 331–342.

22 B. C. Garrett, G. K. Schenter and A. Morita, Molecular simulations of the transport of molecules across the liquid/vapor interface of water, *Chem. Rev.*, 2006, **106**(4), 1355–1374.

23 J. Alejandre, D. J. Tildesley and G. A. Chapela, Molecular-dynamics simulation of the orthobaric densities and surface-tension of water, *J. Chem. Phys.*, 1995, **102**(11), 4574–4583.

24 J. P. Ryckaert, G. Ciccotti and H. J. C. Berendsen, Numerical-integration of Cartesian equations of motion of a system with constraints-molecular-dynamics of N-alkanes, *J. Comput. Phys.*, 1977, **23**(3), 327–341.

25 D. Chandler, Interfaces and the driving force of hydrophobic assembly, *Nature*, 2005, **437**, 640–647.

26 D. Chandler, Hydrophobicity: Two faces of water, *Nature*, 2002, **417**(6888), 491–491.

27 K. Lum, D. Chandler and J. D. Weeks, Hydrophobicity at small and large length scales, *J. Phys. Chem. B*, 1999, **103**(22), 4570–4577.

28 G. Strobl, *The physics of polymers-concepts for understanding their structures and behavior*, Springer, 1996.

29 G. Nagayama and T. Tsuruta, A general expression for the condensation coefficient based on transition state theory and molecular dynamics simulation, *J. Chem. Phys.*, 2003, **118**(3), 1392–1399.

30 L. X. Dang and B. C. Garrett, Molecular mechanism of water and ammonia uptake by the liquid/vapor interface of water, *Chem. Phys. Lett.*, 2004, **385**(3–4), 309–313.

31 A. Morita, M. Sugiyama, H. Kameda, S. Koda and D. R. Hanson, Mass accommodation coefficient of water: Molecular dynamics simulation and revised analysis of droplet train/flow reactor experiment, *J. Phys. Chem. B*, 2004, **108**(26), 9111–9120.

32 R. Vacha, P. Slavicek, M. Mucha, B. J. Finlayson-Pitts and P. Jungwirth, Adsorption of atmospherically relevant gases at the air/water interface: Free energy profiles of aqueous solvation of N-2, O-2, O-3, OH, H_2O, HO_2, and H_2O_2, *J. Phys. Chem. A*, 2004, **108**(52), 11573–11579.

33 J. Vieceli, M. Roeselova and D. J. Tobias, Accommodation coefficients for water vapor at the air/water interface, *Chem. Phys. Lett.*, 2004, **393**(1–3), 249–255.

34 J. Buajarern, L. Mitchem and J. P. Reid, Manipulation and characterization of aqueous sodium dodecyl sulfate/sodium chloride aerosol particles, *J. Phys. Chem. A*, 2007, **111**(50), 13038–13045.

35 J. R. Lawrence, S. V. Glass and G. M. Nathanson, Evaporation of water through butanol films at the surface of supercooled sulfuric acid, *J. Phys. Chem. A*, 2005, **109**(33), 7449–7457.

36 T. Tsuruta and G. Nagayama, Molecular dynamics studies on the condensation coefficient of water, *J. Phys. Chem. B*, 2004, **108**(5), 1736–1743.